



# The Atmospheric Chemistry Experiment (ACE): Aerosol and gas analysis from orbit<sup>☆</sup>

P.F. Bernath<sup>a,b,\*</sup>

<sup>a</sup> Department of Chemistry and Biochemistry, Old Dominion University, Norfolk, VA, 23529, USA

<sup>b</sup> Department of Chemistry, University of Waterloo, Waterloo, Ontario, N2L 3G1, Canada

## ARTICLE INFO

### Keywords:

Satellite remote sensing  
Low-Earth orbit  
Fourier transform spectroscopy  
Clouds and aerosols  
Trace gases  
Infrared spectroscopy

## ABSTRACT

The ACE (Atmospheric Chemistry Experiment) satellite has been in orbit since August 2003. The primary ACE instrument is a high-resolution infrared Fourier transform spectrometer (ACE-FTS) that uses the Sun as a light source to measure atmospheric composition during sunrise and sunset (solar occultation). The long ACE time series allows changes in atmospheric composition to be measured. For example, ACE-FTS monitors changes in the abundance of halogenated gases associated with the Montreal Protocol on Substances that Deplete the Ozone Layer. More recently, infrared transmittance spectra of clouds and aerosols (e.g., polar stratospheric clouds and sulfate aerosols) have been measured. These particles can be characterized by fitting their infrared extinction to determine size and composition.

## 1. Introduction

The Atmospheric Chemistry Experiment (ACE) is a small Canadian satellite launched by NASA in August 2003 [1,2]. Early in the mission, ACE was reviewed from an analytical chemistry perspective [1] (“analytical chemistry from orbit”). For the 10th anniversary on orbit, a book was published [2] reviewing ACE history, hardware, operations and achievements (*The Atmospheric Chemistry Experiment ACE at 10: A Solar Occultation Anthology*). In 2017, the ACE mission was comprehensively reviewed [3] covering hardware, software, operations, and science results. In this 2023 review, a brief overview of the mission will be presented from an analytical perspective, followed by science highlights for the last 5–6 years.

ACE (also known as SCISAT) is a small satellite (Fig. 1) [1–3] that is 1.12 m in diameter and has a mass of 152 kg. It powered by a solar panel on the front of the spacecraft that always points towards the Sun and provides 75 W (orbit average) of power. The satellite bus (spacecraft exclusive of the instruments) was made in Winnipeg, Manitoba, by Magellan Aerospace. The primary instrument is a high resolution infrared Fourier transform spectrometer (ACE-FTS) built by ABB in Quebec City. The ACE-FTS has a spectral resolution of 0.02 cm<sup>-1</sup> in the 750–4400 cm<sup>-1</sup> region. Inside the FTS are two filtered solar imagers operating at 1.02 μm and 0.525 μm. A small visible-near infrared

instrument called MAESTRO (Measurement of Aerosol Extinction in the Stratosphere and Troposphere Retrieved by Occultation) is also on ACE [3], but this review will focus on results from the FTS and the 1.02 μm imager.

All instruments point at the Sun and operate by solar occultation, i.e., the Sun is used as a light source, the limb of the atmosphere is the sample, and the solar radiation is detected by the instruments on the spacecraft. Measurements are made during sunrise and sunset, and a suntracker feeds the instruments. Exoatmospheric spectra are recorded (reference,  $I_0$ ) and a series of atmospheric spectra are recorded as the Sun sets or rises ( $I$ ). A series of atmospheric transmittance spectra of the limb are calculated ( $\tau = I/I_0$ ) and modeled on the ground to provide altitude profiles of molecular concentrations using the Beer-Lambert law.

The satellite has a circular orbit at an altitude of 650 km (at launch) inclined by 73.9° to the equator. It is sinking at about 1 km/year due to air friction. There is one sunrise and one sunset each orbital period of 97.6 min which provide a maximum of 30 occultations each day (15 sunrises and 15 sunsets). The orbit concentrates measurements at high latitudes in the Arctic and Antarctic but provides global coverage about every 2 months (see Figure 6 in Ref. [3]).

<sup>☆</sup> Note for production: this review paper is for the VSI: Air Particles and Gases.

\* Department of Chemistry and Biochemistry, Old Dominion University, Norfolk, VA, 23529, USA.

E-mail address: [pbernath@odu.edu](mailto:pbernath@odu.edu).

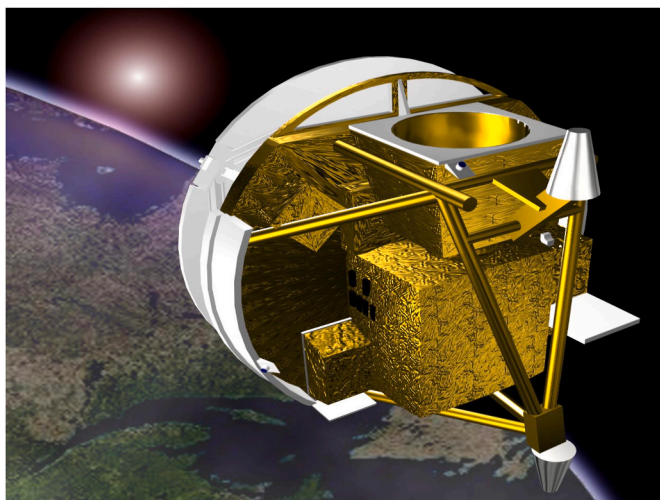


Fig. 1. ACE satellite on orbit.

## 2. ACE-FTS and retrievals

The main instrument on ACE is a Michelson interferometer (ACE-FTS) [3] that uses cube corner retroreflectors. The interferometer has a maximum optical path difference of  $\pm 25$  cm, corresponding to an instrument sampling of  $0.02\text{ cm}^{-1}$  ( $0.5/\text{maximum optical path difference}$ ). The circular input aperture gives a field-of-view of  $1.25\text{ mrad}$  or about  $3\text{ km}$  vertical resolution on the atmospheric limb. There are two photovoltaic infrared detectors, InSb and MCT (mercury cadmium telluride), that measure the interferogram as the optical path changes. The detectors are cooled to about  $80\text{ K}$  by a passive cooler that points to deep space (on the top in Fig. 1). The interferograms are digitized and sent to ground using a microwave link. At the University of Waterloo, the location of the ACE Science Operations Center, the interferograms are Fourier-transformed into spectra.

ACE-FTS infrared spectra have a continuum signal-to-noise ratio of more than 300 over much of the  $750\text{--}4400\text{ cm}^{-1}$  spectral range. For version 4.1/4.2 of the FTS processing [4], altitude profiles of 44 molecules have been retrieved,  $\text{H}_2\text{O}$ ,  $\text{O}_3$ ,  $\text{N}_2\text{O}$ ,  $\text{NO}$ ,  $\text{NO}_2$ ,  $\text{HNO}_3$ ,  $\text{N}_2\text{O}_5$ ,  $\text{H}_2\text{O}_2$ ,  $\text{HO}_2\text{NO}_2$ ,  $\text{O}_2$ ,  $\text{N}_2$ ,  $\text{SO}_2$ ,  $\text{HCl}$ ,  $\text{HF}$ ,  $\text{ClO}$ ,  $\text{ClONO}_2$ ,  $\text{CFC-11}$ ,  $\text{CFC-12}$ ,  $\text{CFC-113}$ ,  $\text{COF}_2$ ,  $\text{COCl}_2$ ,  $\text{COFCl}$ ,  $\text{CF}_4$ ,  $\text{SF}_6$ ,  $\text{CH}_3\text{Cl}$ ,  $\text{CCl}_4$ ,  $\text{HCFC-22}$ ,  $\text{HCFC-141b}$ ,  $\text{HCFC-142b}$ ,  $\text{HFC-134a}$ ,  $\text{HFC-23}$ ,  $\text{CO}$ ,  $\text{CH}_4$ ,  $\text{CH}_3\text{OH}$ ,  $\text{H}_2\text{CO}$ ,  $\text{HCOOH}$ ,  $\text{C}_2\text{H}_2$ ,  $\text{C}_2\text{H}_6$ ,  $\text{OCS}$ ,  $\text{HCN}$ ,  $\text{CH}_3\text{C(O)CH}_3$ ,  $\text{CH}_3\text{CN}$ , PAN ( $\text{CH}_3\text{C(O)OONO}_2$ ), high and low altitude  $\text{CO}_2$  [5]. The most recent processing v.5.2,

released in early 2023, has 46 molecules with the addition of  $\text{HOCl}$  [6],  $\text{HFC-32}$  ( $\text{CH}_2\text{F}_2$ ) [7], and line-of-sight winds from molecular Doppler shifts [8].

Molecular retrievals begin by deriving a temperature/pressure profile and tangent heights (instrument pointing) from spectral features and a numerical weather model [4,9]. From 5 to 18 km, temperature and pressure are taken from the Canadian weather forecast model [4,9]. The tangent heights of these low altitude spectra are unknown because of atmospheric refraction so are retrieved using  $\text{N}_2$  collision-induced absorption. For 18–60 km, the  $\text{CO}_2$  concentration is fixed using a climatology and pressures, temperatures and tangent heights are determined from  $\text{CO}_2$  absorption [4]. Above 60 km, refraction is negligible so pointing is known, and  $\text{CO}_2$  concentrations can be retrieved along with temperature and pressure.

The volume mixing ratio (VMR, fractional abundance) profiles of molecules [4] are determined by holding the temperature/pressure fixed and then calculating each measured spectrum with a “forward” model using line parameters and absorption cross sections (for larger molecules) mainly from the HITRAN database [10]. The atmosphere is divided into 150 spherical layers (shells) that are  $1\text{ km}$  thick. The spectra are calculated using the Beer-Lambert law taking refraction into account along the ray path to the Sun through the layers. To save computer time, each molecule is retrieved individually making use of a carefully selected set of spectral “microwindows”, i.e., short spectral segments containing characteristic absorption feature(s). The VMRs of each molecule are adjusted to minimize the residuals (observed minus calculated spectra) over a selected altitude range [4].

## 3. Recent science highlights

### 3.1. Trends in atmospheric composition

The ACE data record begins in February 2004, after instrument commissioning was finished. The 19-year record (to date) of ACE observations allows trends in atmospheric composition to be measured. Increases in greenhouse gases including  $\text{CO}_2$ ,  $\text{CH}_4$ ,  $\text{N}_2\text{O}$ , etc., are associated with climate change [5].

Of particular interest are halogen-containing gases associated with the Montreal Protocol on Substances that Deplete the Ozone Layer (<https://ozone.unep.org/treaties/montreal-protocol>). Absorption of sunlight by ozone in the stratosphere protects us from deleterious UV radiation. The Montreal Protocol has banned the production of CFCs (chlorofluorocarbons), and their temporary replacements, HCFCs (hydrochlorofluorocarbons), that have shorter atmospheric lifetimes are

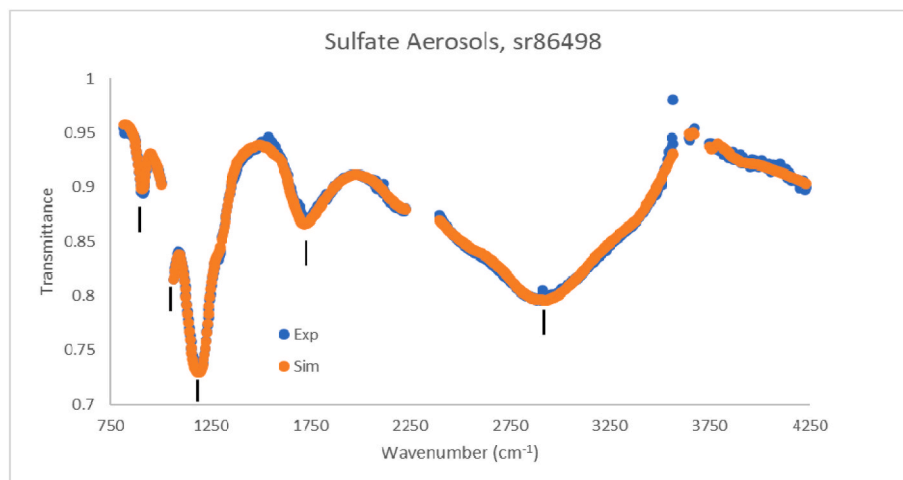


Fig. 2. Sulfate aerosol spectrum from the Raikoke eruption observed at a tangent height of  $22.9\text{ km}$  from the occultation sr86498 (sr is for sunrise and 86498 is the orbit number since launch) on 2 September 2019 at  $26.69^\circ\text{ N}$  latitude and  $47.97^\circ\text{ W}$  longitude [17].

also nearly phased out. HCFCs contain chlorine, which still destroy stratospheric ozone, are being replaced by HFCs (hydrofluorocarbons). Long-lived HFCs do not destroy stratospheric ozone but are powerful greenhouse gases so they in turn are being phased out according to the Kigali Amendment to the Montreal Protocol.

ACE measures global distributions as a function of altitude for the main CFCs, HCFCs and HFCs [5]. These organic source gases are photolyzed in the stratosphere and ultimately make HCl [11] and HF, which ACE also monitors. HCl is slowly decreasing because of the success of the Montreal Protocol in reducing the production of long-lived chlorine-containing gases. Every four years, the World Meteorological Organization/United Nations Environment Programme prepares a report on the state of the ozone layer. The most recent assessment report [12], *Scientific Assessment of Ozone Depletion: 2022*, uses ACE trend data in Chapter 1 on Update on Ozone-Depleting Substances (ODSs) and Other Gases of Interest to the Montreal Protocol and in Chapter 2 on Hydrofluorocarbons (HFCs).

### 3.2. Stratospheric impact of volcanic eruptions

Ash and gases emitted by volcanic eruptions are mainly confined to the tropospheric. However, plumes from large volcanic eruptions reach the stratosphere, and their effects can linger for months and occasionally for years. Volcanic ash particles are relatively large and settle out of the stratosphere within a few days.  $\text{SO}_2$  has a lifetime of about one month in the stratosphere [13] and is converted to sulfate aerosol by reaction with the OH free radical. Sulfate aerosols are droplets of sulfuric acid that have typical lifetimes of about 3 months.

Sulfate aerosols cool the surface of the Earth by scattering sunlight back to space and warm the stratosphere by absorbing outgoing thermal radiation from the surface [14]. Stratospheric chemistry is also altered by large volcanic eruptions, which can deplete ozone. Sulfate aerosols also act as seed particles for the formation of polar stratospheric clouds, which catalyze the destruction of polar ozone in the springtime.

ACE detects stratospheric plumes from volcanoes by measuring enhancements in  $\text{SO}_2$  VMRs [13], increased extinction at  $1.02 \mu\text{m}$  from the ACE imagers [13,15,16], and from the infrared transmittance spectra of sulfate aerosols [15,16]. These infrared spectra (e.g., Fig. 2 from the Raikoke volcano) can be used to characterize sulfate aerosol particles from volcanic eruptions. The Raikoke volcano, located on the Kuril Islands in far eastern Russia, erupted violently on June 21, 2019 with a plume that reached the stratosphere [15].

The observed transmittance spectra (Fig. 2) of sulfate aerosols are obtained by removing all gas phase features to leave “residual” spectra. These spectra are then simulated [15–17] using the Beer-Lambert law and optical constants for sulfuric acid from of Lund Myhre et al. [18]. A log-normal particle size distribution was assumed [17] with the width  $S$  (standard deviation in  $\ln(r)$  space, with  $r$  the radius) fixed to 1.3, and a fixed temperature of 213 K obtained from the retrieved air temperature. The particle extinction coefficients (scattering and absorption) were calculated using the Oxford Mie scattering codes for spherical particles (<http://eodg.atm.ox.ac.uk/MIE/index.html>). The simulation (Fig. 2) that matched the observation had a fitted median radius of  $0.23 \mu\text{m}$ , a composition of 75.1% by weight sulfuric acid, and a column density of  $1.6 \times 10^8$  particles/cm<sup>2</sup>.

In Fig. 2, the blue points are the experimental observations and the orange points are calculated as described above. The residual ACE spectrum has been corrected for artefacts by dividing by a nearby reference spectrum. These artefacts are mainly from nitric acid because the spectroscopic data are incomplete. The short vertical lines are characteristic spectral features associated with sulfuric acid and are described in more detail in Refs. [15–17].

On Jan. 15, 2022, the Hunga Tonga-Hunga Ha’apai volcano erupted violently with an explosive power comparable to the largest nuclear test explosions [16]. This underwater Tonga volcano is located in the South Pacific at  $20.54^\circ$  S latitude and  $175.38^\circ$  W longitude. The Tonga

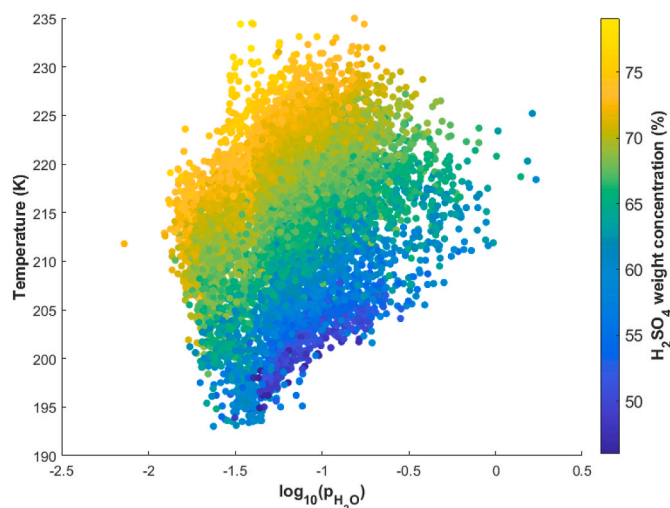


**Fig. 3.** Observed composition of sulfate aerosols. The  $\text{H}_2\text{SO}_4$  concentration (weight %) using the color scale on the right as a function of temperature (K) and  $\log_{10}(\text{H}_2\text{O}$  vapor pressure in Pa). Points from Tonga, Raikoke and Nabro volcanic eruptions are included [16].

eruption reached a record altitude of 57 km in the lower mesosphere, and injected large quantity of  $\text{H}_2\text{O}$  and  $\text{SO}_2$  into the stratosphere. Within a few weeks, the  $\text{SO}_2$  was converted into stratospheric sulfate aerosols which have persisted for more than one year in the Southern Hemisphere.

ACE has made extensive spectral observations to characterize the Tonga aerosol plume focusing on the chemical composition. The climate impact of sulfate aerosols depends on their composition, which is customarily assumed to be 75% by weight  $\text{H}_2\text{SO}_4$ . In fact, the measured composition varies substantially depending primarily on two thermodynamic variables: temperature and  $\text{H}_2\text{O}$  vapor pressure (Fig. 3). Fig. 3 includes points from Tonga, Raikoke and Nabro volcanic plumes. In Fig. 3, the vertical axis is the temperature in K and the horizontal axis is the base 10 logarithm of the  $\text{H}_2\text{O}$  vapor pressure in Pa. Each point corresponds to a measured spectrum with the retrieved composition in weight percent of  $\text{H}_2\text{SO}_4$  indicated by the color, with the color scale on the right.

As temperature decreases and water vapor pressure increases, the sulfuric acid concentration decreases. A multiple linear regression of the weight % of sulfuric acid as function of temperature and the logarithm of the water vapor pressure provides a convenient empirical formula to predict the composition of volcanic sulfate aerosol plumes [16].

### 3.3. Polar stratospheric clouds

Polar stratospheric clouds catalyze the destruction of polar ozone. Ozone-depleting substances such as CFCs are photolyzed in the stratosphere and release Cl atoms which can destroy ozone. Fortunately, most of this chlorine ends up in the form of HCl and  $\text{ClONO}_2$  reservoir molecules, which do not react with ozone. However, in the winter, the Arctic and the Antarctic stratosphere become so cold that nitric acid and water condense to form PSCs (polar stratospheric clouds). These PSCs catalyze the release of chlorine from reservoir molecules by heterogeneous reactions such as  $\text{HCl} + \text{ClONO}_2 \rightarrow \text{Cl}_2 + \text{HNO}_3$ . When sunlight returns in the spring, the liberated chlorine destroys stratospheric ozone and causes the Antarctic “ozone hole”.

PSCs are in the form of solid nitric acid trihydrate (NAT), supercooled ternary solutions of nitric acid and sulfuric acid (STS), and ice. ACE has recorded infrared transmittance spectra of PSCs and as expected has identified characteristic spectra of these three PSCs (and their mixtures) [19]. In addition, a common new fourth spectral type of PSC was identified (Fig. 4): supercooled nitric acid (SNA), i.e., a binary

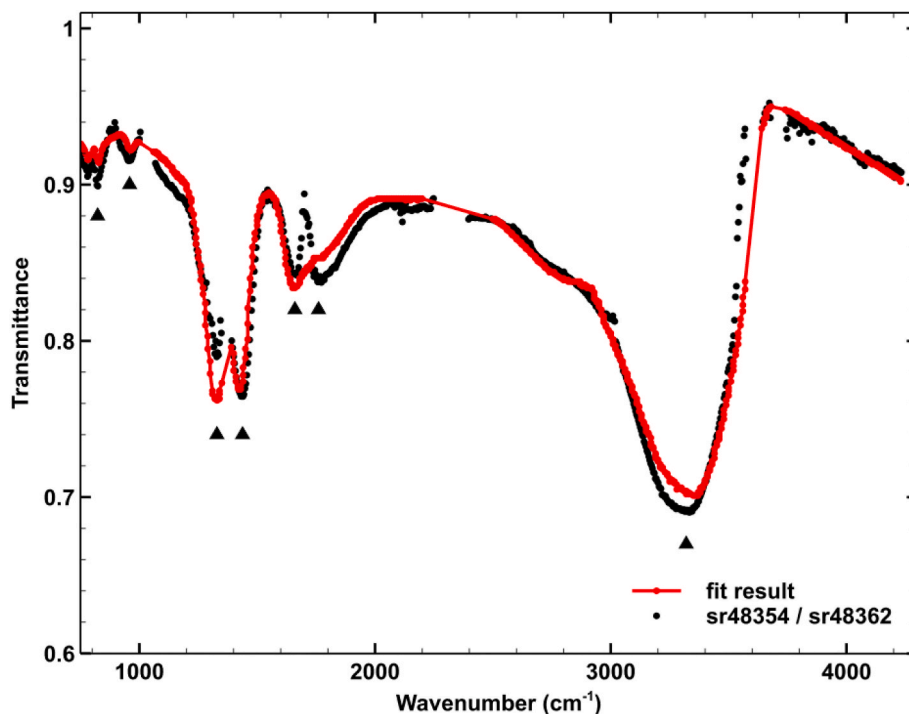


Fig. 4. Spectrum of supercooled nitric acid observed in Antarctica at a tangent altitude of 22.0 km from occultation sr48358 on 5 August 2012 at 67.16° S latitude and 47.69° W longitude. The spectrum has been divided by the reference spectrum sr48362. Triangles mark characteristic nitric acid features [19].

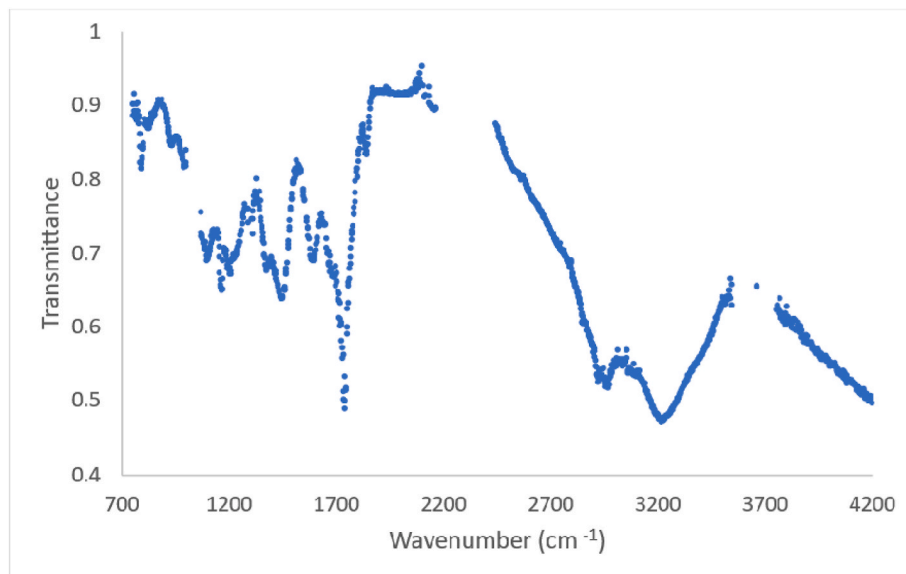


Fig. 5. Stratospheric smoke spectrum observed at a tangent height of 17.6 km from occultation ss88712 (ss is sunset and 88712 is the orbit number) on 30 January 2020 at 47.50° S latitude and 163.16° E longitude from the Australian black summer [17].

solution of nitric acid and water.

The spectrum in Fig. 4 was simulated with the optical constants of Norman et al. [20] assuming spherical particles of a single radius. The fitted parameters are a median radius of 0.393  $\mu\text{m}$ , 47.5% by weight  $\text{HNO}_3$ , and a column density of  $1.65 \times 10^8$  particles/ $\text{cm}^2$ .

### 3.4. Stratospheric smoke and ozone

Smoke and molecular emissions from wildfires are usually confined to the troposphere. Intense wildfires, however, can produce pyrocumulonimbus (pyroCb) clouds that inject smoke and organic molecules

into the stratosphere. Climate change is increasing the frequency of large wildfires and ACE has been measuring spectra of pyroCbs [21]. The largest pyroCbs have occurred during the Australian “Black Summer” fires during late December 2019 and January 2020. Enhanced concentrations of about ten gases including CO, HCN and  $\text{CH}_3\text{OH}$  were measured near 18 km altitude in the fire plume [21]. The infrared transmittance spectrum of wildfire smoke in the stratosphere was recorded (Fig. 5).

Surprisingly, spectra of stratospheric smoke have many absorption features (Fig. 5). The most prominent are assignable to C=O carbonyl stretching ( $1740 \text{ cm}^{-1}$ ), C–H stretching ( $2962 \text{ cm}^{-1}$ ) and O–H stretching

(3225  $\text{cm}^{-1}$ ) modes, consistent with a surface carboxylic acid group. In addition, there is a water librational mode at 800  $\text{cm}^{-1}$  and OH stretching mode as a shoulder at 3420  $\text{cm}^{-1}$  due to surface water. Stratospheric smoke particles therefore have hydrated acidic surfaces.

The Australian black summer fires were so extreme that they altered the chemistry of the stratosphere [22]. The smoke particles catalyzed the destruction of stratospheric ozone by a previously unknown surface chemistry. Changes in the midlatitude southern hemisphere concentrations of chlorine-containing gases were dramatic: HCl decreased and ClONO<sub>2</sub>, HOCl and ClO increased. Other changes included an increase in the formaldehyde abundance and a decrease in nitrogen dioxide. Although midlatitude stratospheric temperatures are too high to form PSCs, there are some similarities between polar ozone chemistry and the chemistry on smoke particles. The ozone declines are related mainly to chlorine chemistry with HCl being converted to more reactive compounds such as ClO. However, smoke increases ClONO<sub>2</sub> and PSCs decrease ClONO<sub>2</sub>. Clearly more laboratory work is needed to study reactions on the surface of smoke particles.

### 3.5. Atlas of spectra of aerosols and clouds

Although the ACE mission has focused mainly on trace gases, in recent years the study of “residual” spectra with the gases removed has been very productive. Overall, nine different types of aerosol and cloud spectra have been identified (polar mesospheric clouds, nitric acid trihydrate, supercooled sulfuric/nitric acid ternary solutions, supercooled nitric acid, PSC ice, cirrus clouds, stratospheric smoke from fires, volcanic ash, and sulfate aerosols) and collected in an atlas [17,19]. Many of these cloud and aerosol spectra have been modeled as described above for spherical particles such as sulfate aerosols. However, solid particles such as NAT, ice (PSCs, cirrus clouds and polar mesospheric clouds) are not spherical, and their spectra were simulated using the Mishchenko and Travis T-matrix code [23]. The T-matrix code calculates the extinction of a distribution of prolate or oblate ellipsoidal particles. Although these solid particles are not actually ellipsoidal, this modeling approach matches the observations reasonably well.

## 4. Conclusions

The ACE satellite is still working well after nearly 20 years on orbit. ACE measures changes in atmospheric composition as a function of altitude on a global scale. For example, by measuring the abundances of halogenated gases that cause stratospheric ozone depletion, ACE monitors the effectiveness of the Montreal Protocol. For example, ACE measures global trends in concentrations of CFCs, HCFCs, HFCs and their final reaction products, HCl and HF. ACE also measures all major greenhouse gases (CO<sub>2</sub>, CH<sub>4</sub> and N<sub>2</sub>O) and aerosols that are responsible for climate change. Recently ACE has begun to measure the spectra of clouds and aerosols by removing gas phase features and calculating residual spectra. These infrared spectra can be used to characterize the particles by determining their composition and size. Of particular interest are stratospheric sulfate aerosols from major volcanic eruptions. Simulation of their spectra provides a reliable estimate of composition which is needed to calculate their climate impact. Polar stratospheric clouds are associated with the destruction of polar ozone (Antarctic ozone hole) and ACE infrared spectra provide a detailed view of their composition and size.

### Declaration of competing interest

The author declares that he has no known competing financial interests or personal relationships that could have appeared to influence the work reported in this paper.

## Data availability

Data is freely available on ACE website or the data for the figures are available in the publications cited.

## Acknowledgements

Funding is provided by the Canadian Space Agency (9F045-200575/001/SA), NASA SAGE-III-ISS Team (80NSSC21K1194) and NASA Atmospheric Composition Modeling and Analysis Program (80NSSC23K0999). PB acknowledges RB for productive discussion.

## References

- [1] P.F. Bernath, Atmospheric Chemistry Experiment (ACE): analytical chemistry from orbit, *Trends Anal. Chem.* 25 (2006) 647–654, <https://doi.org/10.1016/j.trac.2006.05.001>.
- [2] P. Bernath (Ed.), *The Atmospheric Chemistry Experiment ACE at 10: A Solar Occultation Anthology*, A. Deepak Publishing, Hampton, VA, 2013.
- [3] P.F. Bernath, The Atmospheric Chemistry Experiment (ACE), *J. Quant. Spectrosc. Rad. Transfer* 186 (2017) 3–16, <https://doi.org/10.1016/j.jqsrt.2016.04.006>.
- [4] C.D. Boone, P.F. Bernath, D. Cok, S.C. Jones, J. Steffen, Version 4 retrievals for the Atmospheric Chemistry Experiment Fourier transform spectrometer (ACE-FTS) and imagers, *J. Quant. Spectrosc. Rad. Transfer.* 247 (2020), 106939, <https://doi.org/10.1016/j.jqsrt.2020.106939>.
- [5] P.F. Bernath, J. Crouse, R.C. Hughes, C.D. Boone, The Atmospheric Chemistry Experiment Fourier transform spectrometer (ACE-FTS) version 4.1 retrievals: trends and seasonal distributions, *J. Quant. Spectrosc. Rad. Transfer.* 259 (2021), 107409, <https://doi.org/10.1016/j.jqsrt.2020.107409>.
- [6] P.F. Bernath, R. Dodangogode, C.D. Boone, J. Crouse, HOCl retrievals from the Atmospheric Chemistry Experiment, *J. Quant. Spectrosc. Rad. Transfer.* 264 (2021), 107559, <https://doi.org/10.1016/j.jqsrt.2021.107559>.
- [7] R. Dodangogode, P.F. Bernath, C.D. Boone, J. Crouse, J.J. Harrison, The first remote-sensing measurements of HFC-32 in the Earth's atmosphere by the Atmospheric Chemistry Experiment Fourier transform spectrometer (ACE-FTS), *J. Quant. Spectrosc. Rad. Transfer.* 272 (2021), 107804, <https://doi.org/10.1016/j.jqsrt.2021.107804>.
- [8] C.D. Boone, J. Steffen, J. Crouse, P.F. Bernath, Line of sight winds and Doppler effect smearing in ACE-FTS solar occultation measurements, *Atmosphere* 12 (2021) 680, <https://doi.org/10.3390/atmos12060680>.
- [9] C.D. Boone, P.F. Bernath, Tangent height determination from the N<sub>2</sub>-continuum for the Atmospheric Chemistry Experiment Fourier transform spectrometer, *J. Quant. Spectrosc. Rad. Transfer.* 238 (2019), 106481, <https://doi.org/10.1016/j.jqsrt.2019.04.033>.
- [10] I.E. Gordon, et al., The HITRAN2020 molecular spectroscopic database, *J. Quant. Spectrosc. Rad. Transfer* 277 (2022), 107949, <https://doi.org/10.1016/j.jqsrt.2021.107949>.
- [11] P. Bernath, A.M. Fernando, Trends in stratospheric HCl from the ACE satellite mission, *J. Quant. Spectrosc. Rad. Transfer* 217 (2018) 126–129, <https://doi.org/10.1016/j.jqsrt.2018.05.027>.
- [12] World Meteorological Organization (WMO), Scientific assessment of ozone depletion: 2022, in: GAW Report No. 278, 509, WMO, Geneva, 2022. <https://csl.noaa.gov/assessments/ozone/2022/>.
- [13] W.D. Cameron, P. Bernath, C. Boone, Sulfur dioxide from the Atmospheric Chemistry Experiment (ACE) satellite, *J. Quant. Spectrosc. Rad. Transfer.* 258 (2020), 107341, <https://doi.org/10.1016/j.jqsrt.2020.107341>.
- [14] S. Kremser, L.W. Thomason, M. von Hobe, M. Herrman, T. Deshler, C. Timmreck, et al., Stratospheric aerosol – Observations, processes, and impact on climate, *Rev. Geophys.* 54 (2016) 278–335, <https://doi.org/10.1002/2015RG000511>.
- [15] C.D. Boone, P.F. Bernath, K. LaBelle, J. Crouse, Stratospheric aerosol composition observed by the Atmospheric Chemistry Experiment following the 2019 Raikoke eruption, *J. Geophys. Res.: Atmosphere* 127 (2022), e2022JD036600, <https://doi.org/10.1029/2022JD036600>.
- [16] P. Bernath, C. Boone, A. Pastorek, D. Cameron, M. Lecours, Satellite characterization of global stratospheric sulfate aerosols released by Tonga volcano, *J. Quant. Spectrosc. Rad. Transfer* 299 (2023), 108520, <https://doi.org/10.1016/j.jqsrt.2023.108520>.
- [17] M.J. Lecours, P.F. Bernath, J.J. Sorensen, C.D. Boone, R.M. Johnson, K. LaBelle, Atlas of ACE spectra of clouds and aerosols, *J. Quant. Spectrosc. Rad. Transfer* 292 (2022), 108361, <https://doi.org/10.1016/j.jqsrt.2022.108361>.
- [18] C.E. Lund Myhre, D.H. Christensen, F.M. Nicolaisen, C.J. Nielsen, Spectroscopic study of aqueous H<sub>2</sub>SO<sub>4</sub> at different temperatures and compositions: variations in dissociation and optical properties, *J. Phys. Chem. A* 107 (2003) 1979–1991, <https://doi.org/10.1021/jp026576n>.
- [19] M. Lecours, P. Bernath, C. Boone, J. Crouse, Infrared transmittance spectra of polar stratospheric clouds, *J. Quant. Spectrosc. Rad. Transfer.* 294 (2023), 108406, <https://doi.org/10.1016/j.jqsrt.2022.108406>.
- [20] M.L. Norman, J. Qian, R.E. Miller, D.R. Worsnop, Infrared complex refractive indices of supercooled liquid HNO<sub>3</sub>/H<sub>2</sub>O aerosols, *J. Geophys. Res.* 104 (1999) 30571–30584, <https://doi.org/10.1029/1999JD900902>.
- [21] C.D. Boone, P.F. Bernath, M.D. Fromm, Pyrocumulonimbus stratospheric plume injections measured by the Atmospheric Chemistry Experiment Fourier transform

- spectrometer (ACE-FTS), *Geophys. Res. Lett.* 47 (2020), e2020GL088442, <https://doi.org/10.1029/2020GL088442>.
- [22] P. Bernath, C. Boone, J. Crouse, Wildfire smoke destroys stratospheric ozone, *Science* 375 (2022) 1292–1295, <https://doi.org/10.1126/science.abm5611>.
- [23] M.I. Mishchenko, L.D. Travis, Capabilities and limitations of a current FORTRAN implementation of the T-matrix method for randomly oriented, rotationally symmetric scatterers, *J. Quant. Spectrosc. Rad. Transfer* 60 (1998) 309–324, [https://doi.org/10.1016/S0022-4073\(98\)00008-9](https://doi.org/10.1016/S0022-4073(98)00008-9).